

Thermal expansion of free-standing graphene: benchmarking semi-empirical potentials

This content has been downloaded from IOPscience. Please scroll down to see the full text.

2014 J. Phys.: Condens. Matter 26 185401

(<http://iopscience.iop.org/0953-8984/26/18/185401>)

View [the table of contents for this issue](#), or go to the [journal homepage](#) for more

Download details:

IP Address: 193.49.32.117

This content was downloaded on 01/07/2015 at 12:08

Please note that [terms and conditions apply](#).

Thermal expansion of free-standing graphene: benchmarking semi-empirical potentials

Y Magnin¹, G D Förster¹, F Rabilloud¹, F Calvo¹, A Zappelli² and C Bichara²

¹ Institut Lumière Matière, UMR 5306 Université Claude Bernard Lyon 1–CNRS, Université de Lyon, 10 Rue Ada Byron, F69622 Villeurbanne Cedex, France

² CINaM, CNRS and Aix-Marseille University, Campus de Luminy, Case 913, F13288 Marseille, France

E-mail: magnin@cinam.univ-mrs.fr

Received 16 January 2014, revised 28 February 2014

Accepted for publication 4 March 2014

Published 22 April 2014

Abstract

The thermodynamical properties of free-standing graphene have been investigated under constant zero pressure as a function of temperature using Monte Carlo simulations. A variety of atomistic models have been used, including the simple three-body Stillinger potential and a series of bond-order many-body potentials based on the Tersoff–Brenner seminal models, with recent reparametrizations dedicated to graphene, extensions to medium-range or long-range dispersion corrections. In addition, we have also tested a tight-binding potential in the fourth-moment approximation. The simulations reveal significant discrepancies in the in-plane lattice parameter and the thermal expansion coefficient, which despite showing monotonically increasing variations with temperature, can be positive, negative or change sign at moderate temperature depending on the potential. Comparison with existing experimental and theoretical data obtained from complementary approaches indicates that empirical potentials limited to nearest-neighbour interactions give rather dispersed results, and that van der Waals corrections generally tend to flatten the variations of the in-plane lattice constant, in contradiction with experiment. Only the medium-range corrected potentials of Los and Fasolino, as well as the tight-binding model in the fourth-moment approximation, are reasonably close to the reference results near room temperature. Our results suggest that classical potentials should be used with caution for thermal properties.

Keywords: graphene, Monte Carlo simulations, atomistic models, thermal expansion coefficient

(Some figures may appear in colour only in the online journal)

1. Introduction

Graphene, the two-dimensional allotrope of carbon, has recently risen as a highly promising electronic material for its many unusual transport properties in comparison to 3D semiconductors [1–4]. Thermal excitation induces large-scale ripples perpendicular to the graphene layer [5], a phenomenon absent in the hydrogenated material (graphane) [6] but with some influence on the electronic properties [7, 8]. As a consequence, this corrugation leads to a decrease of the in-plane

graphene surface causing a negative in-plane thermal expansion coefficient (TEC) $\alpha = (1/a) da/dT$ at low temperatures (with a the in-plane lattice parameter) and a corresponding positive out-of-plane contribution [5]. At higher temperatures, the possibility that α becomes positive, which would indicate an increase in a with temperature, and the associated microscopic mechanisms of the structural deformation both remain unclear.

Experimentally, the TEC of a suspended graphene layer can be derived from the in-plane lattice parameter a as a function

of temperature T . Bao and co-workers [9] measured the sagging of a suspended graphene layer by scanning electron microscopy and related it to α for temperatures between 300 K and 400 K. They observed that α changes from negative to positive values at around 350 K. Using a nanoelectromechanical resonator, Singh and co-workers [10] found a negative α in the temperature range of 30–300 K. Finally, Yoon and co-workers [11] observed a negative α up to 400 K from Raman spectroscopy measurements. However, it should be noted that this latter determination was inferred after removing the contribution of the biaxial strain of the substrate, as obtained from independent theoretical calculations by Mounet and Marzari based on density functional perturbation theory (DFPT) [12]. Using a quasiharmonic approximation based on the phonon modes computed at the density functional theory (DFT) level, these authors predicted a negative α up to 2500 K [12]. A similar approach was followed by Huang and Zeng [13] who confirmed that α should be negative at least up to 800 K. Pozzo and co-workers [14] performed molecular dynamics (MD) simulations at the DFT level in the isothermal–isobaric NPT ensemble and found a negative α up to 2000 K. Using a non-equilibrium Green's function approach, Jiang and co-workers [15] reported that α changes from negative to positive at about 600 K. Finally, Zakharchenko and co-workers [16] performed Monte Carlo (MC) simulations in the NPT ensemble with the LCBOP-II potential of Los *et al* [17], and found that the change in sign may occur near 900 K.

As with most materials, the use of atomistic potentials for modelling graphene is motivated by the possibility to perform large-scale simulations that give access to quantities and mechanisms hard to address by simulations based on first-principles or by experiments alone. In addition, the successful development of an atomistic potential contributes to improving our understanding of the underlying physics and chemistry that are responsible for bonding and emerging properties. Recent simulations of graphene materials have notably probed melting [18], elasticity [19] and thermomechanical properties [20], ripple [21] and wrinkle formation [22, 23] as well as thermal conductivity [24].

Among the various generic potentials existing for modelling materials at the atomistic level [25–27], many models have been developed specifically for carbon at different degrees of realism and sophistication [17], [28–38]. Although these potentials are all able to handle pure sp^2 bonding, and with some rare exceptions [36, 37], they were generally not aimed at modelling graphene but, at best, graphite [17, 30, 31]. Some authors have also reparametrized existing potentials specifically for graphene [39]. Simulations employing tight-binding (TB) quantum approaches have also been carried out, mostly for addressing electronic transport properties [40] rather than thermodynamical issues.

To date, except for the LCBOP-II potential [18, 19, 23], the general performance of most atomistic potentials for quantifying thermal expansion coefficients of graphene remains poorly documented. It is the goal of the present paper to calculate the thermal expansion coefficients of free-standing graphene monolayers by means of Monte Carlo simulations at finite temperature, under constant zero pressure, for various

atomistic potentials that are appropriate to sp^2 carbon. In particular, we wish to classify among those potentials which compare best to existing reference data from experiment or alternate theories, and to determine the relative importance of the ingredients of those potentials in terms of type (empirical versus bond-order), range (number of neighbours, account or neglect of dispersion forces), and of course parametrization.

We have thus carried out extensive simulations of graphene sheets in a broad temperature range, focusing on the structural properties of the lattice parameter a and the in-plane TEC α , but also, albeit in less detail, the average bond length d_{CC} , and the amplitude Δz of thermal corrugation. Our results indicate that all potentials used exhibit monotonically increasing variations for α , in qualitative agreement with reference data at moderate and high temperatures. Only for potentials with a long-range van der Waals contribution does the lattice parameter exhibit very weak variations with temperature, giving rise to vanishingly small values for the TEC. However, the decreasing variations of α at low temperatures and the occurrence of a minimum in $\alpha(T)$ at moderate temperatures are not reproduced by any of the potentials tested here, at variance with aforementioned theoretical works [12–15] in which phonons were described quantum mechanically, but also with experimental data for graphite [41, 42].

The article is organized as follows. Section 2 gives an overview of the various interatomic potentials used in the present work, emphasizing their common and contrasted features. Section 2.6 details the simulation protocol and discusses the application of our methodology to the structural properties of free-standing graphene monolayers at finite temperatures and zero pressure. The results are presented in section 3, emphasizing the similarities and discrepancies among the atomistic potentials, or between them and experimental or theoretical reference data. The possible causes for these discrepancies are discussed in section 4. Finally, we conclude in section 5 by summarizing the main results and suggesting future research.

2. A menagerie of potentials

Several atomistic potentials have been used in the present work, differing in their functional form or parametrization scheme. These potentials are briefly described in the present section, highlighting their similarities and differences. For the complete details and parameter sets, we refer the reader to the original publications. In the following, we denote by $\mathbf{R} = \{\mathbf{r}_i\}$ the set of atomic coordinates, and by $E(\mathbf{R})$ the potential energy of configuration \mathbf{R} .

2.1. Stillinger–Weber

The Stillinger–Weber (SW) potential [28], selected mostly for its historical merit, was originally developed for silicon and later adapted for carbon [43]. In the absence of an external field, the SW potential reads

$$E(\mathbf{R}) = \sum_{i<j} f^{\text{cut}}(r_{ij}) [V^{\text{rep}}(r_{ij}) + V^{\text{att}}(r_{ij})] + \sum_{i<j<k} g(r_{ij}, r_{ik}, \theta_{ijk}), \quad (1)$$

where r_{ij} is the distance between atoms i and j , $f^{\text{cut}}(r)$ is a cut-off function that truncates the interaction at a given number of neighbours, $V^{\text{rep}}(r)$ and $V^{\text{att}}(r)$ being the repulsive and attractive contributions to the pair energy. The energy also involves the three-body function g of the angle θ_{ijk} , which is constructed in order to favour specific angles θ_0 thereby mimicking sp^3 ($\theta_0 = 109.47^\circ$) or sp^2 ($\theta = 120^\circ$) hybridizations. In the present work, parameters of the SW potential are taken from Abraham and Batra [43].

2.2. Empirical bond-order potentials

In contrast to the fully empirical SW potential, bond-order potentials (BOPs) are rooted in the chemical pseudopotential theory proposed by Abell [44] and have a connection with the embedded atom method used for metals [45]. BOPs treat electronic binding as an effective pair potential, but with a many-body function describing the influence of the local environment around each atom on individual bonds. Several BOPs have been selected for the present study, differing in their specific functional form, their account of a variable set of neighbours, specific modifications to account for medium- or long-range corrections as well as dedicated terms to deal with chemical reactivity or changes in hybridization.

The Tersoff potential [29] writes the potential energy as

$$E(\mathbf{R}) = \sum_i \sum_{i < j} f^{\text{cut}}(r_{ij}) [V^{\text{rep}}(r_{ij}) - \bar{B}_{ij} V^{\text{att}}(r_{ij})] \quad (2)$$

$$\bar{B}_{ij} = \frac{b_{ij} + b_{ji}}{2}$$

where b_{ij} is a many-body contribution to the i -side of the bond-order \bar{B}_{ij} that involves a sum over all neighbours k to i of a function of r_{ik} , r_{jk} , and the angle θ_{ijk} between atoms i , j , and k . The bond strength thus depends both on the coordination and the bond angle, and is chosen in such a way as to disfavor overcoordination.

The Brenner potential [46] was initially developed as an extension of the Tersoff model to account for chemical reactivity in hydrocarbons. The functional form of the Brenner potential is similar to that of Tersoff, but contains in the bond-order expression b_{ij} an additional conjugation term aimed to correct for the inherent overbonding of radicals.

In a more recent effort, Brenner *et al* [32] have extended this potential to better describe a greater variety of systems and chemical reactions, using different expressions for the bond-order, a change in the angular function at small angles, and an extra four-body torsional term. The resulting reactive empirical bond-order (REBO) potential has an improved training set granting a much higher ability to mimic chemical reactions in extended hydrocarbons.

The Tersoff [29], Brenner [46] and REBO [32] potentials have in common that interactions are only counted between nearest-neighbours. They have been used here with the original sets of parameters taken from [29] and [46] (second set) and [32], respectively. In addition, we have also carried out simulations using more recent parametrizations of the Tersoff and REBO potentials optimized specifically for graphene by Lindsay and Broido (LB) [39] to reproduce the phonon dispersion curves near

room temperature. The corresponding potentials are denoted as Tersoff–LB and REBO–LB in what follows.

2.3. Medium-range corrected bond-order potentials

The incapability of early BOPs to properly describe multi-layer graphitic materials was noted by Los and Fasolino [33], who proposed a new potential extending the Brenner model beyond first neighbours through a double Morse potential at intermediate distances. In this so-called LBOP approach, the effective pair energy $V(r_{ij})$ from the Brenner potential is complemented by a medium-range contribution accounting for non-covalent bonding, the transition between the covalent and non-covalent ranges being ruled by a switching function $S(r_{ij})$ that screens at short distances:

$$E(\mathbf{R}) = E^{\text{Brenner}}(\mathbf{R}) + S(r_{ij}) V^{\text{NC}}(r_{ij}). \quad (3)$$

The additional parameters of the LBOP potential were adjusted to *ab initio* data, ensuring that graphite and diamond are also both well described.

More recently, the same authors have proposed a different model in which the short-range covalent part is significantly altered for improved flexibility, the medium-range behaviour is also described using a Morse potential but without any switching function [17, 34]. More importantly, this so-called long-range carbon bond-order potential (LCBOP) was entirely reparametrized to better reproduce structural, energetic, and elastic properties of various bulk carbon materials, including graphite. Both the LBOP and LCBOP models of Los and Fasolino are used in the present work.

2.4. Long-range corrected bond-order potentials

The versions of the BOPs proposed by Los and Fasolino are significantly more accurate and transferable [17] but they are also more involved. Despite the extension to neighbours beyond the first ones, the LBOP and LCBOP models remain of finite range owing to the exponential attenuation of the attractive potential. In particular, the dispersion interaction acting at long distances was not considered, even though it is known to be physically responsible for the binding between graphene sheets in graphite. At least two groups have attempted to correct for this deficiency in the standard BOPs by adding specific dispersion interactions.

The GEEBOD force field developed by the Goddard group [30] extends Brenner's original potential to include an additional Lennard–Jones (LJ) potential between all pairs of atoms, each LJ interaction being weighted by a many-body function that smoothly vanishes when the two atoms are covalently bound. Although the GEEBOD potential probably overbinds graphene layers in graphite [33], its most significant shortcoming is its relatively heavy computational cost due to the many-body character and environment dependence of the switching function.

The adaptive intermolecular reactive empirical bond-order (AIREBO) potential of Stuart and co-workers [31] was also developed as an extension of the REBO potential with extra Lennard–Jones interactions between distant atoms. Again, a smooth switching function based on interatomic distances but also involving the local connectivity of the atoms in the pair

was introduced so that covalently bound atoms are not affected. The switching functions used for GEEBOD, AIREBO as well as LBOP significantly contribute to the computational cost of those potentials.

2.5. Tight-binding model within the fourth-moment approximation

We have considered a recently developed tight-binding (TB) model in the fourth-moment approximation (FMA) to the local density of states, as developed by Amara and co-workers to describe the carbon–nickel system [38]. As opposed to the above mentioned potentials, the TB–FMA model relies on a quantum mechanical-based tight-binding approximation of the electronic structure. Hamiltonian matrix elements, parametrized in the Slater–Koster form, are explicitly included, but the time-consuming diagonalization of the matrix is replaced by a Green's function expansion limited to the fourth-moment of the local *s* and *p* electron densities of states. In this approximation, first and second neighbours contribute to the band structure term of the local energy and an empirical repulsive term is added. The cohesive energy in the TB–FMA model is not fully explicit, as it involves evaluating the first moments of the local density of electronic states through continued fraction expansions [38]. The full details and parametrization of the TB–FMA model are given in the original publication [38]. In the present work, the technical improvements proposed by Los *et al* [47] were further employed in order to alleviate a significant part of the computational cost during the elementary Monte Carlo moves. Despite not including long-range dispersion corrections, the TB–FMA model accounts for next-neighbours interactions and is considered as a medium-range model.

Finally, table 1 summarizes the main features of the potentials used in this work in terms of their developer, history, and range of their interactions according to nearest-neighbours (short-range), next-nearest-neighbours (medium-range), and all neighbours (long-range). The reference giving the parameters, and some generic properties about the temperature variations of *a* and the sign and possible sign change of the TEC α , as discussed below, are also listed.

2.6. Computational method

Classical Monte Carlo simulations have been performed in the isothermal–isobaric ensemble to evaluate thermally averaged structural observables of pristine graphene as a function of temperature and under constant zero pressure. The graphene monolayer is assumed to lie at mechanical equilibrium in the $z = 0$ plane of a rhombohedral prism simulation box. Periodic boundary conditions are imposed on *x* and *y* directions in the minimum image convention, while a free boundary is applied on *z*. The two-dimensional simulation cell area is denoted by $S = \sqrt{3}L_xL_y/2$ where L_x and L_y correspond to the edge lengths of the simulation box. Our MC algorithm is standard and consists of alternating random, spherically isotropic atomic moves with global box moves that scale the entire coordinates of all atoms. At zero external pressure the general Metropolis acceptance probability reads [48]

Table 1. Potentials used in the present work, and listed according to their historical development (authors and year published), their nature (empirical, empirical BOP, tight-binding), range (nearest-neighbours or short-range, next-nearest-neighbours or medium-range, with van der Waals corrections or long-range), and reference where the numerical parameters used can be found. The temperature behaviour of the in-plane *a* (decreasing \searrow , increasing \nearrow , non-monotonic $\searrow\nearrow$) and the in-plane TEC (remaining positive +, negative –, or changing sign \rightarrow) in a temperature range in-between 0–2000 K, as discussed in the text, are also given.

Potential	Nature	Range	Reference	<i>a</i>	TEC α
Stillinger-Weber 1985	Empirical	short	[43]	\searrow	–
Tersoff 1989	BOP	short	[29]	$\searrow\nearrow$	\rightarrow
Brenner 1990	BOP	short	[46]	\searrow	–
REBO 2002	BOP	short	[32]	\nearrow	+
Tersoff–LB 2010	BOP	short	[39]	\nearrow	+
REBO–LB 2010	BOP	short	[39]	\nearrow	+
LBOP 2002	BOP	medium	[33]	\searrow	–
LCBOP 2003	BOP	medium	[34]	$\searrow\nearrow$	\rightarrow
GEEBOD 1999	BOP	long	[30]	\searrow	–
AIREBO 2000	BOP	long	[31]	$\searrow\nearrow$	\rightarrow
TB–FMA 2009	TB	medium	[38]	\searrow	\rightarrow

$$\text{acc}(\mathbf{R}_{\text{old}} \rightarrow \mathbf{R}_{\text{new}}) = \min \left\{ 1, \left(\frac{V(\mathbf{R}_{\text{new}})}{V(\mathbf{R}_{\text{old}})} \right)^N \exp(-\beta[E(\mathbf{R}_{\text{new}}) - E(\mathbf{R}_{\text{old}})]) \right\} \quad (4)$$

where $V(\mathbf{R})$ is the volume of configuration \mathbf{R} , $\beta = 1/k_B T$ with k_B the Boltzmann constant.

As is customary in the simulation of liquids dealing with pairwise potentials [48], long-range corrections δV_{lr} were included for the GEEBOD and AIREBO potentials in order to account for the contribution of the van der Waals interactions beyond the box dimensions. This contribution vanishes for all other potentials, and is not relevant at fixed density, but may play a role at fixed pressure because δV_{lr} varies upon box moves. In the present case, neglecting the corrugation at long-range allows us to treat graphene as a uniformly flat distribution of LJ centres beyond the cut-off distance r_c , which yields

$$\delta V_{\text{lr}} = \frac{-\pi N C_6}{\Sigma r_c^4}, \quad (5)$$

for the atomic correction, with Σ the surface density and $C_6 = 4\epsilon\sigma^6$ the dispersion coefficient from the Lennard–Jones expression.

Being a 2D material rippling in 3D space, the definition of the instantaneous volume of a deformed graphene layer is ambiguous. Three approaches have been followed, in which the system is considered as 3D or 2D. In the 3D case, the volume was first evaluated directly from the simulation box (L_x, L_y, L_z) as $V = SL_z = \sqrt{3}L_xL_yL_z/2$. However, L_z being of no physical significance, we have also considered to measure the volume of the graphene layer from its corrugation magnitude $\Delta z = z_{\text{max}} - z_{\text{min}}$, z_{min} and z_{max} being the lowest and highest elevations at the current configuration as depicted in figure 1(a).

Alternatively, we have compared the predictions of those 3D methods with a 2D treatment of graphene assuming that

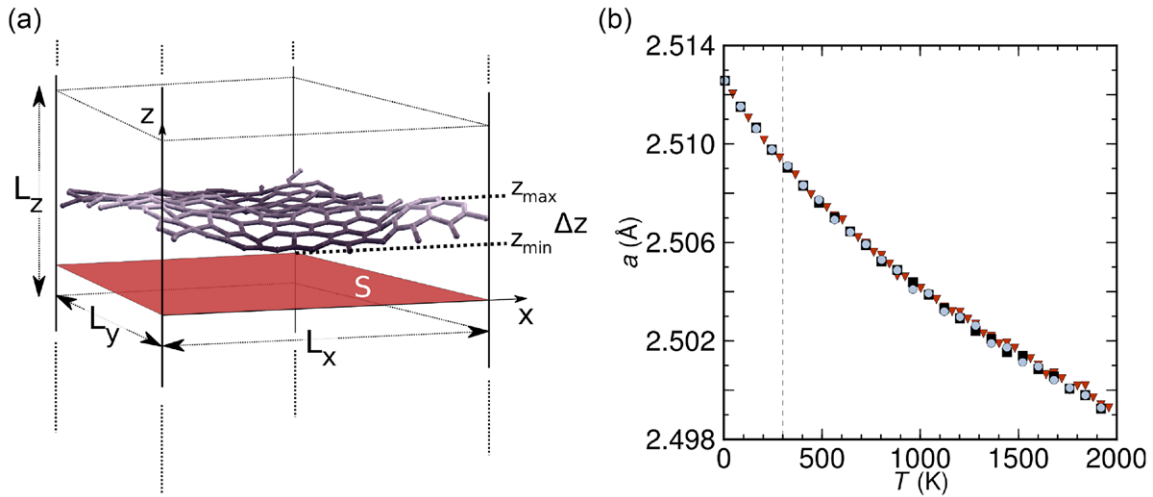


Figure 1. (a) Schematic representation of the simulation box. The blue lattice corresponds to the corrugated graphene monolayer with a corrugation amplitude denoted by $\Delta z = z_{\max} - z_{\min}$. The in-plane graphene surface area S is represented in red. (b) Temperature dependence of the free-standing graphene lattice parameter a under constant zero pressure. Results of the figure were calculated using the Brenner *et al* potential [32]. Red triangles correspond to the 2D scaling procedure, black squares to the 3D scaling procedure using the volume definition $V = SL_z$ and blue circles to the 3D scaling procedure using the volume definition $V^* = S\Delta z$. The vertical dashed line locates $T = 300$ K.

pressure is only exerted laterally, the volume in equation (4) being then replaced by the surface area S .

Those three methods for evaluating the volume of the graphene sheet have been tested for a 200-atom sample with the Brenner potential, and the results shown in figure 1(b) indicate negligible differences among them for the equilibrium lattice parameter $a(T)$, the same conclusions being reached for the magnitude of out-of-plane corrugation $\Delta z(T)$ or the enthalpy $U(T) = \langle E \rangle$ (data not shown). The equivalence of these approaches is due to the separation in scale of the energy contribution due to in-plane and out-of-plane displacements. Based on this comparison, all simulations were carried out using the surface area S as the variable conjugate to pressure in the MC simulations.

Finally, the simulations were performed by varying the simulation box size, including 10×10 , 15×15 , and 20×20 unit cells or 200, 450, and 800 atoms, respectively. No significant differences were found in the resulting out-of-plane bond length d_{CC} or enthalpy $U(T)$. However, increasing the box size was found to slightly decrease the in-plane a , as also reported by Pozzo and co-workers [14], and concomitantly increase the corrugation amplitude Δz , by about 1% between the 200- and 450-atom systems. Such variations were already noticed by Chen and Chrzan [19] who reported similar effects for the LCBOP II potential. They reflect the higher strain experienced by the graphene layer in small cell sizes, as manifested by higher corrugation and a lower in-plane surface area. Considering the computational cost involved in simulating larger samples at various temperatures and with sufficient statistics, we have limited the simulations presented below to the smallest cell size (200 atoms), keeping in mind that the structural observables are the lowest bounds, by a few per cents, of the macroscopically converged limiting values.

3. Results

The simulations carried out with the potentials listed in table 1 spanned the temperature range 0–2000 K by steps of

$\Delta T = 40$ K and consisted of 10^7 MC sweeps for each temperature following 10^7 equilibration sweeps. For the computationally more intensive LBOP [33], GEEBOD [30] and AIREBO [31] potentials, those numbers had to be adjusted to $\Delta T = 80$ K. The statistical uncertainties on a , evaluated from the block averaging technique, typically fall below 0.1% and are omitted for clarity as they are smaller than the depicting symbols. For all simulations, the temperature variations of the in-plane lattice parameter a obtained from averaging out the MC trajectories were fitted using a fourth-order polynomial to yield a smoothly varying TEC α , instead of attempting a numerically much more noisy finite temperature differentiation.

We start by showing in figure 2 the temperature variations of the in-plane a and the in-plane TEC $\alpha = (1/a) da/dT$ obtained in various experiments [9–11] and theoretical investigations [12–15], as taken from the original references.

In the experimental work by Baskin and Meyer [49], a was integrated from the given α , fixing the value of a at 300 K to be 2.459 Å. Quite curiously, this quantity is not strictly reproduced by the theoretical reference data except the DFT calculation of Pozzo and co-workers [14]. Despite these minor variations, all reported reference data exhibit a common monotonic decrease in a with increasing T , in keeping with a negative α in the entire temperature range considered here. The most salient discrepancy among the reference data is related to the sign of the in-plane TEC α , which can either remain negative [10, 11] or change sign [9]. With respect to measurements, theoretical estimates generally underestimate the TEC in magnitude and show a minimum in the range 100–400 K, in qualitative agreement with the Raman spectroscopy experiment [11].

The results obtained in the present work for the simple empirical Stillinger–Weber potential [28] parametrized for graphite by Abraham and Batra [43] have been superimposed in figure 2. They indicate a monotonically decreasing but convex $a(T)$ consistent with a negative but increasing TEC α . Figure 3 depicts the results obtained from the present simulations with

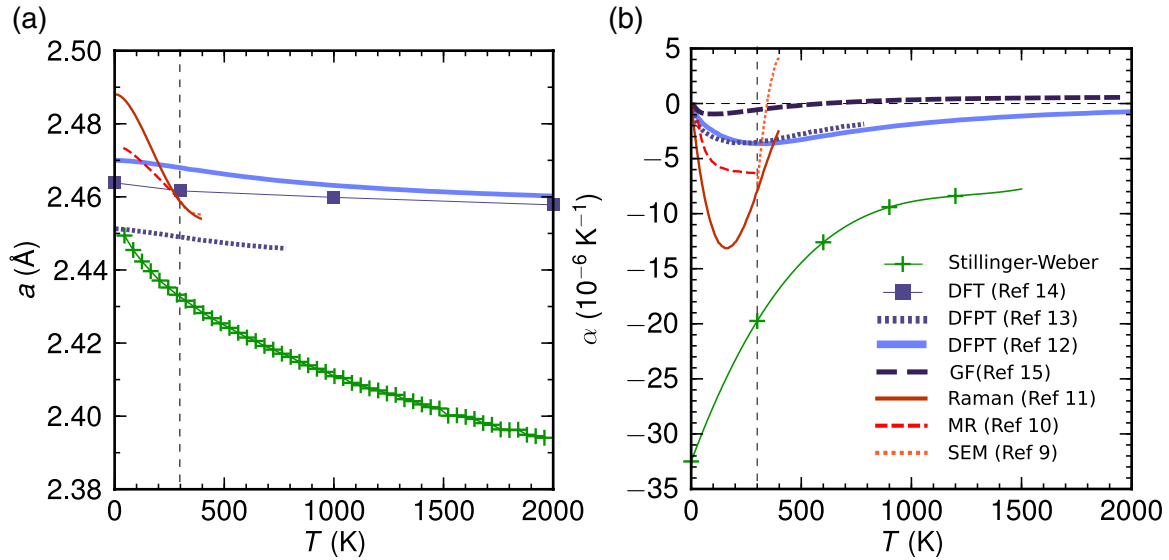


Figure 2. Temperature dependence of (a) the in-plane lattice parameter a obtained for the empirical Stillinger–Weber from the present simulations (green pluses [28, 43]) (b) the corresponding in-plane TEC α . Experimental results obtained from Raman spectroscopy (brown thin solid line [11]), nanomechanical resonator (MR, red thin dashed line [10]) and scanning electron microscopy (SEM, orange dotted line [9]) as well as computational results from density functional theory simulations (DFT, blue squares [14]), density functional perturbation theory calculations (DFPT, light blue solid line [12] and blue dots [13]), and non-equilibrium Green’s function method (GF, dark blue dashed line [15]) are also shown.

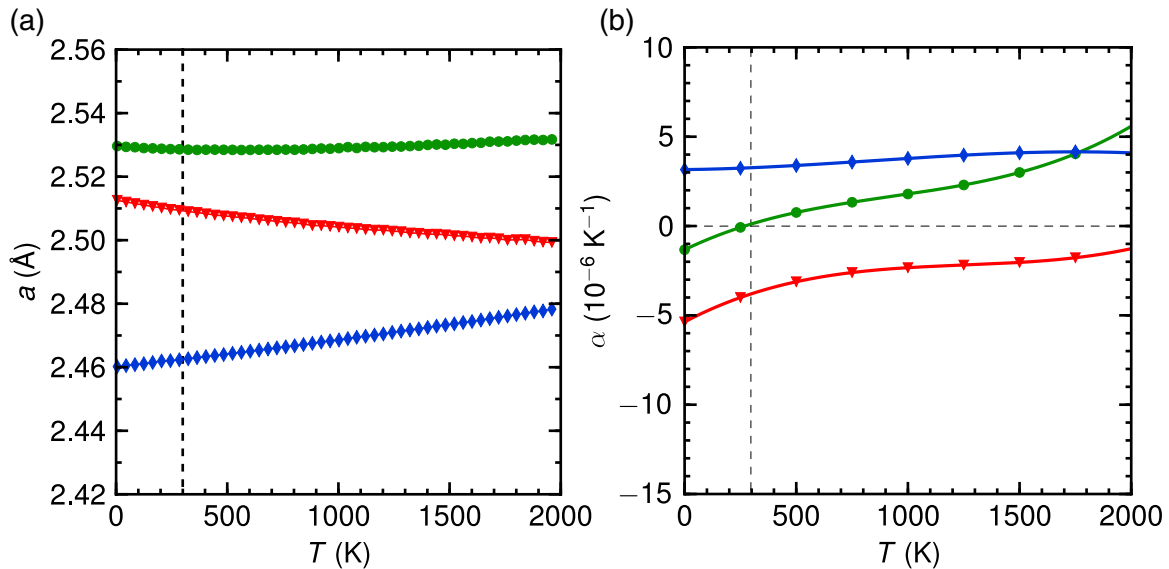


Figure 3. Temperature dependence of (a) the in-plane lattice parameter a obtained from the present MC simulations for the Tersoff (green circles), Brenner (red triangles) and REBO (blue diamonds) potentials and (b) the corresponding in-plane TEC α .

other short-range potentials, as parametrized by Tersoff [29] and Brenner in the original [46] and REBO [32] versions.

These three potentials with their historical sets of parameters exhibit significant discrepancies among one another, with only the Brenner potential showing qualitative agreement with the reference data of figure 2, whereas the Tersoff and REBO models yield a non-monotonic $a(T)$ or a monotonically increasing $a(T)$, respectively. Only the REBO potential gives a reasonable value for a at 300 K, which is a consequence of its more flexible functional form enabling both cohesion energy and lattice parameter to be reproduced.

Lindsay and Broido [39] recently reparametrized the Tersoff and REBO potentials to reproduce the phonon dispersion

curves of graphite. The fitting procedure was carried out within the harmonic approximation valid at low temperature and, as a consequence, those potentials turn out to be unstable at moderate temperatures. The properties obtained with those two potentials in limited temperature ranges are presented in figure 4.

With these new parametrizations, both potentials exhibit monotonically increasing variations in $a(T)$, in contrast with the reference data but consistently with the predictions of the original REBO model. These results highlight the significant dependence of such an essential thermomechanical property as the in-plane lattice parameter a with the atomistic model.

In contrast to the Tersoff and Brenner potentials, the LBOP [33] and LCBOP [34] potentials of Los, Fasolino

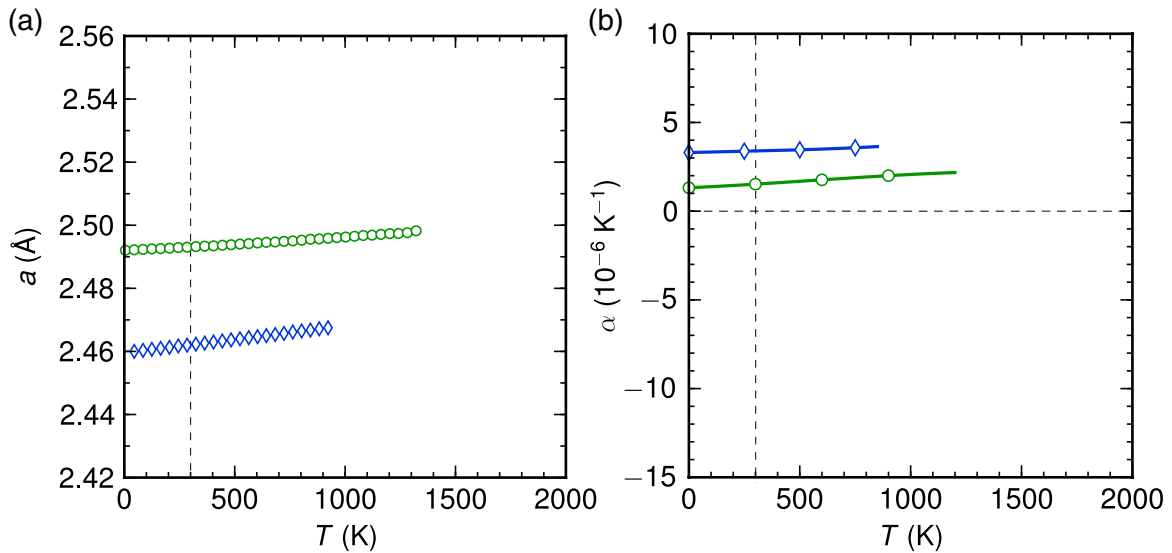


Figure 4. Temperature dependence of (a) the in-plane graphene lattice parameter a obtained from the present MC simulations for the Tersoff-LB (green circles) and REBO-LB (blue diamonds) potentials and (b) the corresponding in-plane TEC α .

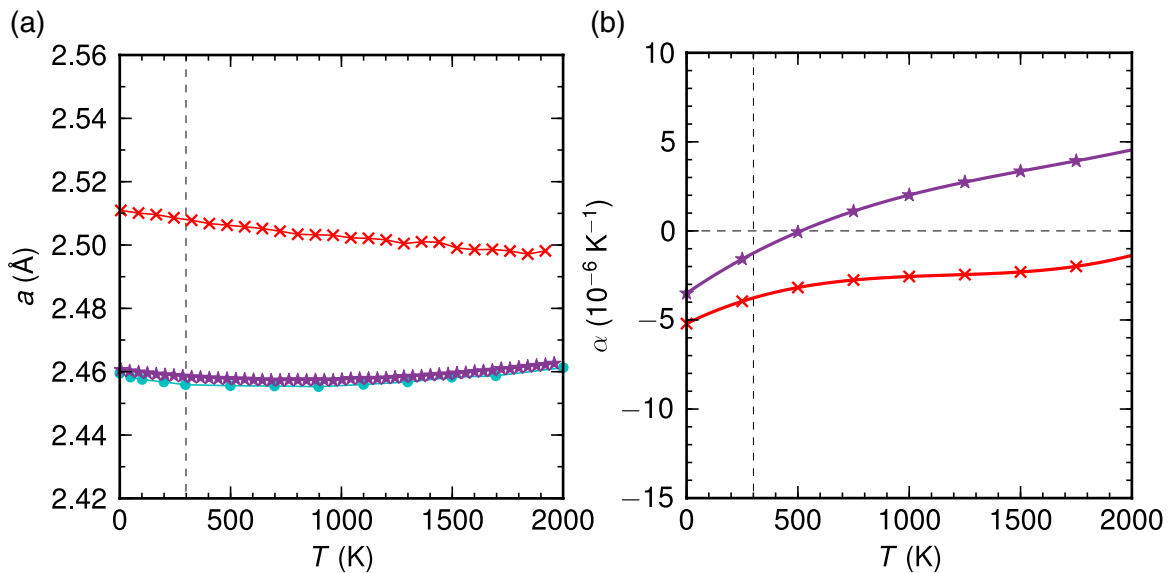


Figure 5. Temperature dependence of (a) the in-plane graphene lattice parameter a obtained from the present MC simulations for the LBOP (red crosses) and LCBOP (purple stars) potentials and (b) the corresponding in-plane TEC α . The variations of a obtained with the LCBOPII potential by Zakharchenko *et al*, also depicted (cyan dots, taken from Reference [16]), are nearly superimposed with the LCBOP data.

and co-workers both extend the interactions beyond nearest-neighbours through medium-range corrections and provide, in principle, a more realistic framework to model graphitic structures. The results obtained with these semi-empirical potentials are depicted in figure 5.

Noteworthy, these two potentials predict different behaviours for both a and α . LBOP yields a monotonically decreasing a and $\alpha < 0$, both in keeping with the results obtained with the Brenner potential from which LBOP derives. In contrast, the in-plane lattice parameter decreases and reaches a minimum with LCBOP, as it does for the similar LCBOPII model [17] but at 900 K instead of 500 K here [16]. The variations obtained here with the LCBOP potential are not surprising, because this potential was partly fitted to reproduce sp^2 carbon allotropes. In particular, the change in sign of α near 500 K is

quantitatively similar to experimental and theoretical data on graphite [12, 41, 42].

Despite still not including long-range dispersive corrections, the TB-FMA model of Amara and co-workers [38] is more physically grounded than all other potentials considered in the present work. As with the LBOP and LCBOP potentials of Los, Fasolino and co-workers, it also belongs to the medium-range category in which interactions are included up to the next-nearest-neighbours. The results obtained with this model, represented in figure 6, indicate non-monotonically increasing variations not only for $a(T)$, with a minimum near 1000 K, but also for $\alpha(T)$, with negative values up to about 800 K and a minimum roughly located in the 100–500 K range (given our numerical fitting procedure used to evaluate α from a).

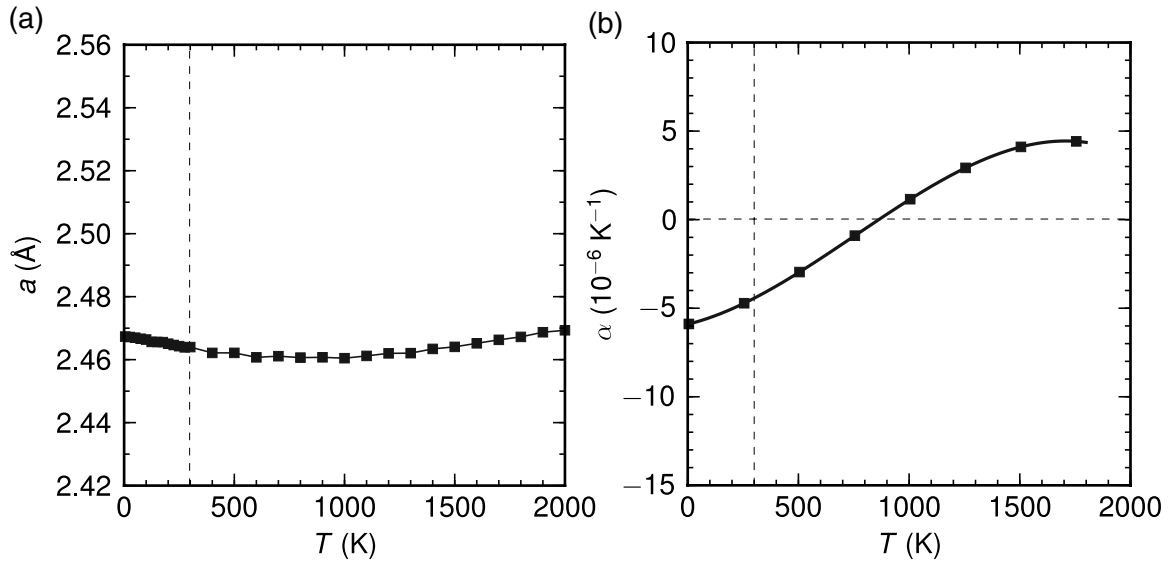


Figure 6. Temperature dependence of (a) the in-plane lattice parameter a obtained from the present MC simulations for the medium-range TB-FMA model [38], and (b) the corresponding in-plane TEC α .

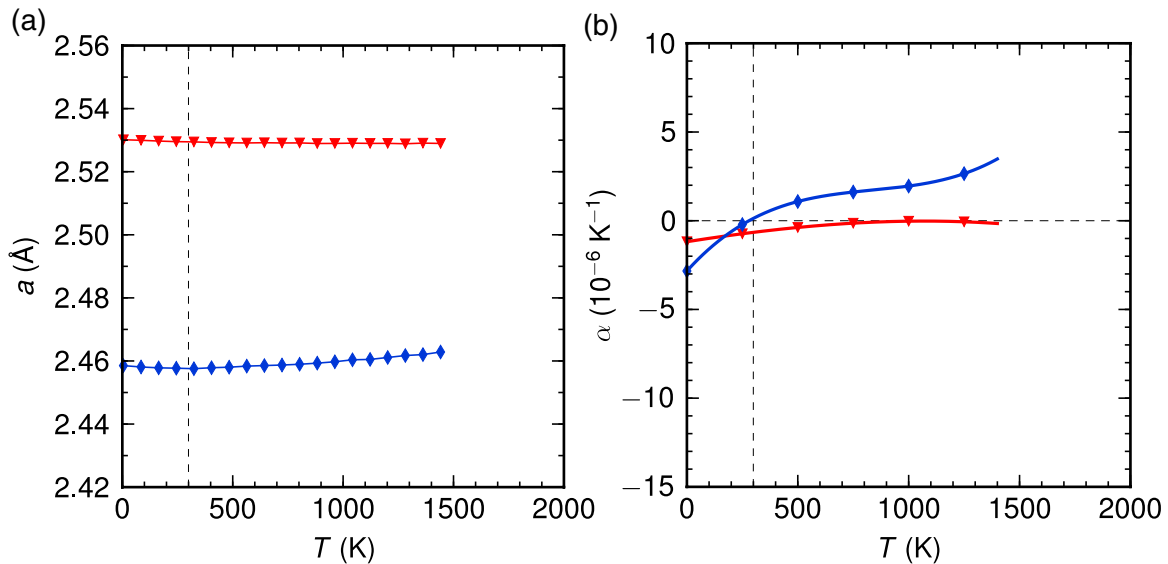


Figure 7. Temperature dependence of (a) the in-plane graphene lattice parameter a obtained from the present MC simulations for the long-range potentials GEEBOD (red triangles [30]) and AIREBO (blue diamonds [31]) and (b) the corresponding in-plane TEC α .

The non-monotonic behaviour of a and the sign change in α exhibited by the TB-FMA model are also reasonably compatible with the experimental [11] and theoretical [12, 13, 15] reference data.

We finish this presentation by giving in figure 7 the results of the long-range corrected potentials GEEBOD and AIREBO. Both potentials show smooth variations in both a and α except at high temperature $T > 1500$ K where they seem to become less stable and have been omitted from the graph. Despite producing rather different in-plane parameters at 0 K, the variations are non-monotonic with shallow minima, the TEC reaching zero near 800 K and 300 K for GEEBOD and AIREBO, respectively. Because GEEBOD is based on the original Brenner potential, the effect of long-range forces can be discriminated by comparing the present results to those of figure 3. The additional Lennard-Jones interaction between non-nearest-neighbours is

clearly not negligible as it contributes to attenuating temperature effects and lowering α in magnitude. Long-range forces have an even stronger effect in the case of AIREBO, a potential that is intimately connected to REBO. Comparing again the results of figures 3 and 7, the dispersion corrections play an especially important role at low temperature, where α turns negative as AIREBO is chosen over REBO. In this specific case, we speculate that the torsion potential introduced in AIREBO to better account for rotational barriers around bonds between sp^3 carbons is not appropriate for graphene, this potential being alternatively maximum and minimum.

Adding long-range forces thus appears more consequential than reparametrizing the short-range potential so that it reproduces phonon dispersion curves. These results show that the thermomechanical behaviour of simulated graphene is not uniquely driven by the $T = 0$ static properties.

4. Discussion

The reference theoretical and experimental results reproduced in figure 2 indicate common trends, but also serious discrepancies. The room temperature lattice constant of 2.459 Å, for instance [51], is better reproduced by the DFT simulations of Pozzo and co-workers [14] than by the quasiharmonic DFPT [12, 13] and GF [15] data, which give rather dispersed values. Among the atomistic potentials used in the present work, REBO, LCBOP and TB-FMA reproduce best this reference value.

The thermal variations of the in-plane TEC α are also sensitive to the potential, even though α always increases monotonically with temperature for all potentials investigated. In the temperature range below 2000 K, α may remain negative (SW, Brenner, LBOP, GEEBOD) or positive (REBO, Tersoff-LB and REBO-LB), or otherwise change sign. However, inspection of figure 2 indicates that, except for the microscopy data of [9], α should generally be trusted as essentially negative. The sign change of α from negative to positive values, also seen with the LCBOPII potential [5], was interpreted by Fasolino and co-workers as a manifestation of a transition from harmonic behaviour at low temperature (soft bending modes giving $\alpha < 0$) to anharmonic behaviour involving tighter stretching modes and their couplings with the other phonons. Such an interpretation is supported by quasiharmonic DFPT calculations [12, 13], which are also in favour of a negative α .

However, this interpretation should also be treated with care, because the Lindsay and Broido reparametrizations of the Tersoff and REBO potentials [39] to fit the phonon dispersion curves of graphite both give $\alpha > 0$. Therefore, having a correct harmonic description does not ensure negative α . A recent theoretical work based on elasticity theory [50] further indicates that anharmonicities alone can lead to $\alpha < 0$, hence we are led to conclude that the value of α and the presence of a sign change at finite temperature depends primarily on the anharmonic couplings rather than on how well the phonons are described. These conclusions could be rationalized using classical perturbation theory, which at first order would yield a linearly varying a and a constant α , whose sign depends on the third and fourth energy derivatives at the equilibrium geometry [51].

A more significant difference between the reference data and the entire set of results obtained here with atomistic potentials is the presence of a minimum in $\alpha(T)$ located between approximately 100 K (GF data from [15]) and 300 K (DFPT results from [12, 13]), a feature completely absent from the present simulations. Noticing that the temperature range considered in this work is below the Debye temperature of graphite, this non-monotonic behaviour is likely connected to the quantum mechanical nature of low-temperature phonons manifested as exponential (rather than linear) attenuation of thermodynamical functions, whereas all present simulations treated nuclear motion as classical. However, it should be noticed that the DFPT approaches treated a and d_{CC} as being proportional to each other, hence the minimum in the TEC α could be a mere artefact originating from this assumption.

Having focused on the thermal expansion coefficient, we have not discussed so far other structural properties more difficult to probe in experiments, and for which reference data to compare

with are more scarce. The average nearest-neighbour carbon-carbon distance $d_{CC}(T)$, for instance, is found to increase linearly with temperature for all potentials studied, only the slope and static value differing among the models (data not shown). These results agree with those obtained by Pozzo and co-workers [14], but are at variance with those reported by Zakharchenko and co-workers [16] who found a minimum in d_{CC} near $T \sim 900$ K with the LCBOPII potential. Considering the similarity between the LCBOP and LCBOPII potentials, these contrasted results again emphasize the high sensitivity of the structural and thermodynamical observables on the details of the model.

Finally, another remarkable result is found in the corrugation amplitude Δz , which is systematically found to be lower when long-range van der Waals interactions are included, both for the GEEBOD and AIREBO potentials in comparison with Brenner and REBO, respectively. The isotropic dispersion correction is attractive at long distances, but out-of-plane deformations are energetically penalized, resulting in the lower value of Δz . Inspecting further the respective influences of the two van der Waals corrections, repeating the simulations without the long-range correction δV_{lr} reveals that this term plays a minor role on the structural and energetic results.

5. Concluding remarks

Meeting the great promises of graphene requires a better understanding of its thermomechanical and structural properties, a task that demands combined experimental efforts and theoretical support. In the present work, we have investigated by means of computer simulation the effects of a finite temperature on the in-plane lattice parameter and its derivative, the thermal expansion coefficient, of free-standing monolayer graphene described by various existing atomistic potentials. The Monte Carlo simulations were carried out in the isothermal-isobaric ensemble at constant zero pressure, and the potentials covered empirical (Stillinger-Weber) to semi-empirical bond-order types (Tersoff, Brenner-REBO possibly corrected at medium- and long-ranges), as well as a model-based on tight-binding theory. Although our selection of potentials is of course not exhaustive, it covers the important category of bond-order potentials that are probably the most popular and widespread among atomistic models, including its recent extensions due to Fasolino and co-workers, and those incorporating dispersion corrections.

While all potentials predict increasing variations of the average C-C distance with increasing temperature, the in-plane lattice parameter exhibits a broad variety of thermal behaviours, with either increasing, decreasing, or non-monotonic variations depending on the potential. The thermal expansion coefficient α resulting from these variations can thus remain positive below 2000 K, in contrast with existing measurements [9–11] or alternative calculations based on quasiharmonic theory [12, 13] that predict $\alpha < 0$, possibly with a sign change below 400 K. Near room temperature, the potentials that come closest to those reference data are the LCBOP and TB-FMA models, but interestingly they were not fitted to reproduce the properties of graphene specifically. In

particular, potentials that incorporate information on graphene such as the phonon dispersion curves do not perform particularly better, and it can thus be concluded that anharmonicities play an important role on the sign and magnitude of the thermal expansion coefficient. Also, adding long-range dispersion corrections in the GEEBOD and AIREBO potentials has a surprisingly large but negative effect with respect to comparison with the reference data. However, the role of dispersion could deserve further attention, because all theoretical studies so far have also neglected those forces in the DFT ingredients they used.

The present results obtained from classical Monte Carlo simulations have in common the monotonic variations exhibited by the thermal expansion coefficient, a feature absent from all reference data. Reproducing those non-monotonic variations would require repeating the simulations in a quantum mechanical framework, using e.g. path-integral methods or the more recent technique of coloured noise thermostats [52, 53] coupled with molecular dynamics.

More importantly, our results call for more experiments in order to clarify the sign and magnitude of α and its possible change at a measurable temperature. The current temperature range appears rather limited, and the contribution of the substrate on which graphene sheets are suspended has to be evaluated more accurately and without any bias or independent evaluation. It would then be particularly useful to extend such measurements to higher temperatures where simulations, when they do, predict that the thermal expansion coefficient becomes positive.

Acknowledgments

We gratefully acknowledge support from the CDC (Centre De Calcul de l'UCP) computing center at Cergy–Pontoise University. This project has been supported by Agence Nationale de La Recherche (ANR NMGM 16-339233).

References

- [1] Castro Neto A H, Guinea F, Peres N M R, Novoselov K S and Geim A K 2009 *Rev. Mod. Phys.* **81** 109
- [2] Novoselov K S, Fal'ko V I, Colombo L, Gellert P R, Schwab M G and Kim K 2012 *Nature* **490** 192
- [3] Weiss N O, Zhou H L, Liao L, Liu Y, Jiang S, Huang Y and Duan X F 2012 *Adv. Mater.* **24** 5782
- [4] Guttinger J, Molitor F, Stampfer C, Schnez S, Jacobsen A, Droscher S, Ihn T and Ensslin K 2012 *Rep. Prog. Phys.* **75** 126502
- [5] Fasolino A 2007 *Nature Mater.* **6** 858
- [6] Costamagna S, Neek-Amal M, Los J H and Peeters F M 2012 *Phys. Rev. B* **86** 041408
- [7] Mariani E and von Oppen F 2008 *Phys. Rev. Lett.* **100** 076801
- [8] Castro E V, Ochoa H, Katsnelson M I, Gorbachev R V, Elias D C, Novoselov K S, Geim A K and Guinea F 2010 *Phys. Rev. Lett.* **105** 266601
- [9] Bao W, Miao F, Chen Z, Zhang H, Jang W, Dames C and Lau C N 2009 *Nature Nanotechnol.* **4** 562
- [10] Singh V, Sengupta S, Solanki H S, Dhall R, Allain A, Dhara S, Pant P and Deshmukh M M 2010 *Nanotechnology* **21** 165204
- [11] Yoon D, Son Y-W and Cheong H 2011 *Nano Lett.* **11** 3227
- [12] Mounet N and Marzari N 2005 *Phys. Rev. B* **71** 205214
- [13] Huang F L and Zeng Z 2013 *J. Appl. Phys.* **113** 083524
- [14] Pozzo M, Alfè D, Lacovig P, Hofmann P, Lizzit S and Baraldi A 2011 *Phys. Rev. Lett.* **106** 135501
- [15] Jiang J W, Wang J S and Li B 2009 *Phys. Rev. B* **80** 205429
- [16] Zakharchenko K, Katsnelson M and Fasolino A 2009 *Phys. Rev. Lett.* **102** 046808
- [17] Los J H, Ghiringhelli L, Meijer E and Fasolino A 2005 *Phys. Rev. B* **72** 214102
- [18] Zakharchenko K V, Fasolino A, Los J H and Katsnelson M I 2011 *J. Phys.: Condens. Matter* **23** 202202
- [19] Chen S and Chrzan D C 2011 *Phys. Rev. B* **84** 195409
- [20] Lajevardipour A, Neek-Amal M and Peeters F M 2012 *J. Phys.: Condens. Matter* **24** 175303
- [21] Singh A K and Hennig R G 2013 *Phys. Rev. B* **87** 094112
- [22] Wang C Y, Mylvaganam K and Zhang L C 2009 *Phys. Rev. B* **80** 155445
- [23] Wang C, Liu Y, Lan L and Tan H 2013 *Nanoscale* **5** 4454
- [24] Hu J, Schiffl S, Vallabhaeni A, Ruan X and Chen Y P 2010 *Appl. Phys. Lett.* **97** 133107
- [25] Erkoç S 1997 *Phys. Rep.* **278** 79
- [26] Brenner D W 2000 *Phys. Status Solidi* **217** 23
- [27] Calvo F, Spiegelman F and Montagnon L 2011 *Encyclopedia of Nanoscience and Nanotechnology* **11** ed Nalwa H S (New York: American Scientific) pp 363
- [28] Stillinger F H and Weber T A 1985 *Phys. Rev. B* **31** 5262
- [29] Tersoff J 1988 *Phys. Rev. B* **37** 6991
- [30] Che J, Çağın T and Goddard I I 1999 *Theor. Chem. Acc.* **102** 346
- [31] Stuart S J, Tutein A B and Harrison J A 2000 *J. Chem. Phys.* **112** 6472
- [32] Brenner D W, Shenderova O A, Harrison J A, Stuart S J, Ni B and Sinnott S B 2002 *J. Phys.: Condens. Matter* **14** 783
- [33] Los J H and Fasolino A 2002 *Comput. Phys. Commun.* **147** 178
- [34] Los J H and Fasolino A 2003 *Phys. Rev. B* **68** 024107
- [35] Los J H, Matsnelson M I, Yazyev O V, Zakharchenko K V and Fasolino A 2009 *Phys. Rev. B* **80** 121405
- [36] Perebeinos V and Tersoff J 2009 *Phys. Rev. B* **79** 241409
- [37] Tewary V and Yang B 2009 *Phys. Rev. B* **79** 075442
- [38] Amara H, Roussel J M, Bichara C, Gaspard J P and Ducastelle F 2009 *Phys. Rev. B* **79** 014109
- [39] Lindsay L and Broido D A 2010 *Phys. Rev. B* **81** 205441
- [40] Jung J and MacDonald A H 2013 *Phys. Rev. B* **87** 195450
- [41] Pierson H O 1993 *Handbook of Carbon, Graphite, Diamond, and Fullerenes: Properties, Processing, and Applications* (Park Ridge, NJ: Noyes)
- [42] Bailey A C and Yates B 1970 *J. Appl. Phys.* **41** 5088
- [43] Abraham F F and Batra I P 1989 *Surf. Sci.* **209** 125
- [44] Abell G C 1985 *Phys. Rev. B* **31** 6184
- [45] Brenner D W 1989 *Phys. Rev. Lett.* **63** 1022
- [46] Brenner D W 1990 *Phys. Rev. B* **42** 9458
- [47] Los J H, Bichara C and Pellenq R J M 2011 *Phys. Rev. B* **84** 085455
- [48] Allen M P and Tildesley D J 1989 *Computer Simulation of Liquids* (Oxford: Oxford University Press)
- [49] Baskin Y and Meyer L J 1955 *Phys. Rev.* **100** 544
- [50] de Andres P L, Guinea F and Katsnelson M I 2012 *Phys. Rev. B* **86** 144103
- [51] Calvo F, Doye J P K and Wales D J 2001 *J. Chem. Phys.* **115** 9627
- [52] Ceriotti M, Bussi G and Parrinello M 2009 *Phys. Rev. Lett.* **102** 020601
- [53] Dammak H, Chalopin Y, Laroche M, Hayoun M and Greffet J-J 2009 *Phys. Rev. Lett.* **103** 190601